

EEG-based Neural Decoding of Gait in Developing Children

Trieu Phat Luu, *Member, IEEE*, David Eguren, *Student Member IEEE*, Manuel Cestari, and Jose L. Contreras-Vidal, *Fellow, IEEE*

Abstract— Neural decoding of human locomotion, including automated gait intention detection and continuous decoding of lower limb joint angles, has been of great interest in the field of Brain Machine Interface (BMI). However, neural decoding of gait in developing children has yet to be demonstrated. In this study, we collected physiological data (electroencephalography (EEG), electromyography (EMG)), and kinematic data from children performing different locomotion tasks. We also developed a state space estimation model to decode lower limb joint angles from scalp EEG. Fluctuations in the amplitude of slow cortical potentials of EEG in the delta band (0.1 – 3 Hz) were used for prediction. The decoding accuracies (Pearson's r values) were promising (Hip: 0.71; Knee: 0.59; Ankle: 0.51). Our results demonstrate the feasibility of neural decoding of children walking and have implications for the development of a real-time closed-loop BMI system for the control of a pediatric exoskeleton.

Keywords—Brain-computer interface, neural decoding, children walking, EEG, EMG, gait.

I. INTRODUCTION

Cerebral Palsy (CP), Spina Bifida (SB) and Spinal Cord Injury (SCI) are major causes of motor function disability in the pediatric population. These conditions can result in reduced mobility and can interfere with a child's ability to achieve critical developmental milestones [1]. Moreover, the socio-economic burden imposed on patients, relatives, and caregivers can be substantial. Neurorehabilitation for the restoration of gait functions after locomotor deficits has been a long-standing focus of researchers and clinical professionals worldwide. Surprisingly, the current understanding of cortical activities during locomotor planning and execution in children is limited, even in typically developing individuals.

Although the roles of central pattern generator networks (CPGs) in generation of the basic synergy of human gait patterns have been postulated [2-4], the roles of supraspinal networks (i.e., including the brainstem, cerebellum, and cortex) must also be involved in the neural control systems to meet additional demands imposed by gait-related tasks [5, 6].

This research was supported by NSF IUCRC BRAIN, Mission Connect – A TIRR Foundation, the University of Houston Cullen College of Engineering, and NSF Awards CNS 1650536

T.P. Luu, D. Eguren, M. Cestari, and J.L. Contreras-Vidal, are with the NSF IUCRC BRAIN Center at the University of Houston, Houston, TX 77204 USA, e-mail: tpluu2207@gmail.com).

These tasks are believed to include the modulation of human locomotion (e.g., gait initiation and termination, gait speed, direction, and spatial orientation), and the integration of multisensory information [7]. The insights into the cortical control of human locomotion gleaned from neuroimaging studies have been limited and lack sufficient temporal solutions for gait analysis. For example, the activation of the supplementary motor cortex and basal ganglia during mental imagery of walking was shown in early studies using blood-oxygen-level dependent (BOLD) signals [8, 9]. Electrophysiological investigations using non-invasive, scalp EEG signals have shown the involvement of the sensorimotor cortex in the control of human gait [10, 11]. Recent non-invasive EEG studies have also revealed differences in electrocortical activities between uphill and level ground walking in humans [12] as well as active versus passive walking in a robotic device [13]. A non-invasive EEG study with an active treadmill demonstrated that user-driven control increases cortical activity [14]. Recent studies have shown the feasibility of decoding lower limb kinematics from non-invasive EEG brain signals using fluctuations in the amplitude of slow cortical potentials in the delta band (0.1 – 3Hz) [15]. Recently, the feasibility of using a real-time, closed-loop BCI for learning to control a walking avatar in a virtual environment has been demonstrated [16-19]. However, the involvement of the brain in locomotor intentions and execution in developing children has not yet been demonstrated.

II. MATERIALS AND METHODS

A. Experimental setup and protocol

All experimental protocols and informed consent were approved by the Institutional Review Board (IRB) at the University of Houston (UH). Written informed consent and parental permission form were obtained from all participants. Five healthy children with ages between four and twelve-year-old with no history of neurological disorder participated in this study. A 64-channel Ag/AgCl active electrode EEG setup (BrainAmp DC and MOVE, Brain Products GmbH, Germany) was used to record wirelessly at 1000 Hz from the face and scalp. Channels TP9, PO9, PO10, and TP10 were removed from the cap and used for electrooculography (EOG) to capture blinks and eye movements; however, these data were excluded from all analyses in this study. The remaining 60 channels were arranged according to the modified 10-20 international system, which was used in our

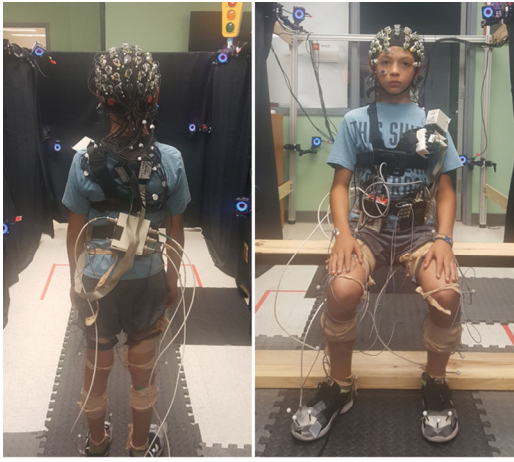


Fig. 1. Experimental setup. Recorded data included EEG, EMG, and kinematics (motion capture system).

previous study [20]. We used a 3-D electrode localization system (BrainVision Captrak, Brain Products GmbH, Germany) to record electrode positions. Surface EMG signals were recorded (Biometrics Ltd, Newport, UK) at 1000 Hz from four sites bilaterally (tibialis anterior, gastrocnemius, rectus femoris, and bicep femoris longus). In addition to the EEG and EMG recordings, lower limb kinematic data were also recorded using a motion capture system (NaturalPoint, Inc. DBA OptiTrack, USA). EEG, EMG and kinematic data were synchronized using our custom hardware and software. Fig. 1. shows the experimental setup in this study.

The participants were instructed to perform four different types of locomotion tasks (i.e., sitting and standing, start and stop overground walking). In the sitting and standing task, the participants completed 20 sit-to-stand and stand-to-sit transitions which were initiated by a visual cue placed in front of the subjects. The session began with the participant standing quietly in an upright posture for 15 seconds. After the quiet standing period, the participant began the self-initiated sit-to-stand and stand-to-sit transitions. The waiting period between the transitions was approximately 10 seconds. The participants were verbally informed when 20 transitions were completed. In the start and stop overground walking session, the participants completed 20 walk-to-stand and stand-to-walk transitions. The session began with the participants standing still for 15 seconds. After the stationary standing period, the participant held the standing position for a period ranging randomly from 10 to 15 seconds before the stand-to-walk transition (indicated by a green light). The participants walked on a 10-meter walkway and were instructed to stop walking at the onset of a red light. The walk-to-stop transition completed a single trial and the participant returned to the starting position. The process continued until 20 trials were completed.

B. Offline EEG signal processing and source localization

The offline EEG analysis was performed using custom software written in Matlab R2016a (The MathWorks, MA) and EEGLAB [21]. Fig. 2 shows a flowchart for the EEG

signal processing pipeline. EOG channels were first removed and the remaining EEG signals (60 channels) were high pass filtered at 0.1 Hz. Corrupted EEG channels were rejected based on criteria in [22]. The remaining EEG channels were then re-referenced by subtracting to their common average.

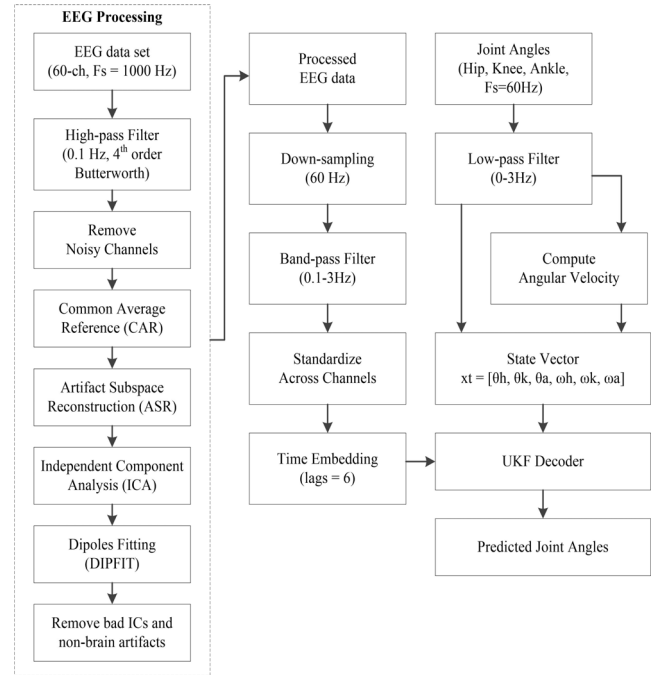


Fig. 2. Flowchart illustrates offline EEG processing and Unscented Kalman Filter used in this study

Next, artifact subspace reconstruction (ASR) was applied to remove high amplitude artifacts (e.g., eye blinks, muscle burst) [23]. After this step, EEG data were down-sampled to 100 Hz and Infomax ICA was applied.

EEG electrodes were aligned to a standard MNI brain model by using 3D position data obtained from a Captrak system. We then computed equivalent current dipole that matched to the scalp projection of each independent component (IC) source by using a standard three-shell boundary element head model included in the DIPFIT toolbox [21]. Only ICs in which the equivalent dipoles explained $> 80\%$ of the variance of the IC scalp projections were retained for further analysis. Next, we visually inspected each IC scalp projection, its equivalent dipole's location, and its power spectra and removed ICs that related to non-brain artifacts (e.g., eye blink/movement, neck muscle). The remaining ICs' activations were band-pass filtered (0.1 – 3 Hz) using a 4th order Butterworth filter. Thus, the EEG features correspond to time-domain amplitude modulated (AM) potentials in the delta band. The EEG data were then standardized by channel by subtracting the mean and dividing by the standard deviation (z-score). The EEG data from the past (60 – 70ms), lags = 6, were used to predict the joint angles. The joint angle data of the right leg were low-pass filtered (0 – 3 Hz) using a 2nd order Butterworth filter. This band is known to cover most power in joint angle signals [24, 25]. Angular velocities were also computed and used in state vector to train the UKF decoder.

C. Unscented Kalman Filter Decoder

Linear decoders (e.g., Wiener filters and Kalman filters) are most commonly used in BCI applications [26, 27]. However, the nonlinearity between neural activities and lower limb movements cannot be captured by such models. The UKF was first introduced by Julier and Uhlman to improve the Kalman filter in the context of nonlinear estimation problems [28]. It handles the nonlinearities using unscented transform (UT), which estimates the statistics of a random variable propagating through a nonlinear function. In this study, the nonlinear system consisted of a movement model (state model) and a neural tuning model (observation model). Details of the UKF algorithm for neural decoding of human walking can be found in our previous studies [29-31]. The state model can be characterized by a matrix F and noise covariance matrix Q , and the observation model can be characterized by a mapping matrix B and noise covariance matrix R . These matrices were obtained by parameter fitting method using training data [32]. After the training process, the UKF was implemented to predict lower limb joint angles from EEG signals. The UKF algorithm started with a prediction step to estimate the current state in the state model:

$$x_t' = Fx_{t-1}, \text{ and } P_t' = FP_{t-1}F^T + Q \quad (1)$$

where $x_t = [\theta_{rh}, \theta_{rk}, \theta_{ra}, \omega_{rh}, \omega_{rk}, \omega_{ra}]^T$ is the state variable at time t , x_t' and P_t' are the predicted state and its covariance, x_{t-1} and P_{t-1} are the previous state and its covariance.

III. RESULTS

A. EEG signal processing and artifact removal

Fig.3. shows rejected ICs in which the equivalent dipoles explained less than 80% of the variance of the IC scalp projections. The number on top of each topoplot represents the index of the ICs and the percentage in parentheses next to the index shows the residual variance (RV) value.

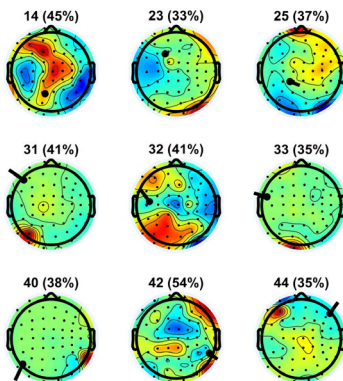


Fig. 3. An example of rejected ICs with a residual variance of more than 20%. The number on the top of each topoplot shows the index of ICs, followed by the residual variance in brackets.

Figs. 4-5. show rejected eye-related and muscle-related artifact ICs, respectively. The dipoles that represent eye-related ICs appear close to the eyes in MRI images (Fig. 4A) and its activities demonstrated by the topoplot (Fig. 4B) are mainly focused on the frontal area. In addition, Fig. 4B shows strong PSD at low frequency and a smooth decreasing of PSD values. The dipoles that represent muscle-related artifacts locate close to the peripheral in the MRI images (Fig. 5A). The spectral power of muscle-related ICs is dominant at high frequencies.

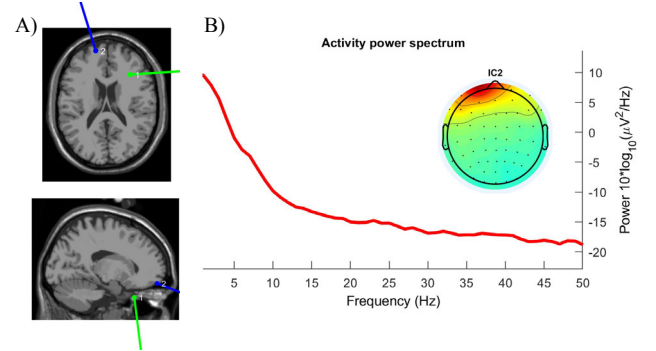


Fig. 4. An example of rejected eye-related artifacts ICs. A) MRI images overlaid with dipoles' location and strength. B) Topoplot and power spectral density of an eye-related IC.

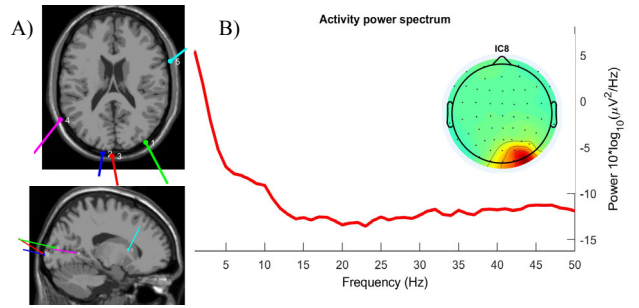


Fig. 5. An example of rejected muscular related artifacts ICs in children EEG data. A) MRI images overlaid with dipoles' location and strength. B) Topoplot and power spectral density of an EMG-related IC.

B. Neural decoder's performance

The UKF decoder was able to predict lower limb joint angles in the sagittal plane from the scalp EEG signals with high accuracy. To quantify the level of accuracy for the neural decoding, Pearson's r values between the measured and the predicted joint angles were computed. Fig. 6. shows the best decoding accuracies with the r values (Hip: 0.71; Knee: 0.59; Ankle: 0.51).

IV. DISCUSSION

In this study, we processed EEG signals and developed a neural decoder (UKF) to predict lower limb joint angles in children walking from EEG data. Our results suggest the feasibility of neural decoding of locomotion in developing children. EEG in the delta band (0.1 – 3 Hz) was used for neural decoding of children walking; thus, the EEG features

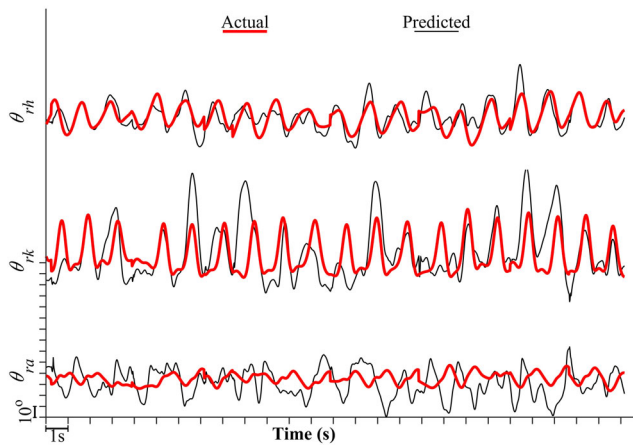


Fig. 6. Neural Decoding of Kinematics: Actual and predicted lower limb joint angles from EEG signals in children walking. Decoding accuracy r -values for hip, knee, and ankle joint are 0.71, 0.59, 0.51, respectively.

correspond to time-domain amplitude modulated (AM) potentials in the delta band. EEG signals in this band have been demonstrated to carry relevant information of human gait. For example, Gwin et al. showed that meaningful changes in EEG during walking or running occur at low frequencies (< 10 Hz) [33]. Slow cortical potentials in the delta band EEG have also been utilized to decode human gait during treadmill walking with a linear decoder and the results were comparable with invasive BCI approaches [26]. Recent studies from Luu et al., have shown high decoding accuracy of a real-time closed loop BCI for human treadmill walking from EEG signal in the delta band [17-19].

The results from this study may lead to the development of a real-time closed-loop BMI for automated gait intention detection in children. The BMI system can be used for the control of an assistive exoskeleton for neurorehabilitation in children with gait deficits. Such novel systems allow volitional control and enhance the level of motor attention from the user during the training process. In this paradigm, the user is in control and engages in the training process, and the user is at the center of the intervention. The current proposal could potentially lead to the development of a novel training paradigm for improving the efficacy of neurological rehabilitation based on a top-down approach. Our future works aim to extend the proposed method to a larger population of typically developing children.

Although promising results for neural decoding of walking in developing children have been demonstrated, several potential challenges must be addressed to develop robust and reliable EEG-based neural decoding of pediatric walking in real-time. First, scalp EEG signals are susceptible to many physiological and non-physiological artifacts (e.g., eye blinks, eye movements, cardiac signal, muscle artifact, and motion-related artifacts) which may impede the decoding accuracy. We used active EEG electrodes to allow higher signal to noise ratio (SNR) in EEG signals and to eliminate the mechanical artifacts induced by the movement of EEG wires and cables. In this study, we implemented ICA and DIPFIT algorithms to remove artifactual components in EEG

signals. This approach is effective in the offline analysis but it is not applicable in real-time applications. To suppress eye-related artifacts in real-time applications, we recommend using a robust filter with EOG signals as reference inputs [34]. Our study focus on slow speed walking at 1mph and the decoder will utilize neural features in the low-frequency band. This design eliminates the effects of muscle artifacts (occurs in 30-1k Hz), line noise (50-60 Hz), and motion artifacts (pronounced effects at normal and fast walking speed). Thus, our decoding methods are robust to the artifactual components of EEG signals.

Second, EEG signals carry not only motor efferent control during human walking, but also multisensory afferent feedback. Extracting meaningful neural features from scalp EEG signals for the decoding of human gait is a non-trivial process. To address this, we use a causal model that predicts the current kinematics from EEG signals prior to the current motor command. Note that there are certain delays in feedback signals associated with the current motor command; therefore, the afferent feedback is modulated in future EEG signals which are not included as inputs in the designed causal model.

Finally, neural signals are highly dynamic [35, 36] and neuroplasticity plays a critical role in developing a robust neural decoder [37]. Neural decoders are typically trained offline by fitting neural signals against actual movements. This approach, however, ignores the neural dynamics from subjects when switching from open-loop to closed-loop BCI and typically results in decreased online performance. Based on previous studies [38, 39] showing that closed-loop decoder adaptation (CLDA) yields performance improvement, it is recommended to train and update the neural decoder at a fixed interval (e.g., one minute).

REFERENCES

1. Calhoun, C.L., J. Schottler, and L.C. Vogel, *Recommendations for mobility in children with spinal cord injury*. Topics in spinal cord injury rehabilitation, 2013. **19**(2): p. 142-151.
2. Calancie, B., et al., *Involuntary stepping after chronic spinal cord injury: Evidence for a central rhythm generator for locomotion in man*. Brain, 1994. **117**(5): p. 1143-1159.
3. Angeli, C.A., et al., *Altering spinal cord excitability enables voluntary movements after chronic complete paralysis in humans*. Brain, 2014. **137**(5): p. 1394-1409.
4. Dimitrijevic, M.R., Y. Gerasimenko, and M.M. Pinter, *Evidence for a spinal central pattern generator in humans*. Annals of the New York Academy of Sciences, 1998. **860**(1): p. 360-376.
5. Nielsen, J.B., *How we Walk: Central Control of Muscle Activity during Human Walking*. The Neuroscientist, 2003. **9**(3): p. 195-204.
6. Grillner, S., et al., *Neural bases of goal-directed locomotion in vertebrates—an overview*. Brain research reviews, 2008. **57**(1): p. 2-12.
7. Rossignol, S., R. Dubuc, and J.-P. Gossard, *Dynamic sensorimotor interactions in locomotion*. Physiological reviews, 2006. **86**(1): p. 89-154.
8. La Fougere, C., et al., *Real versus imagined locomotion: a [18 F]-FDG PET-MRI comparison*. Neuroimage, 2010. **50**(4): p. 1589-1598.
9. Fukuyama, H., et al., *Brain functional activity during gait in normal subjects: a SPECT study*. Neuroscience letters, 1997. **228**(3): p. 183-186.

10. Wieser, M., et al., *Temporal and spatial patterns of cortical activation during assisted lower limb movement*. Experimental brain research, 2010. **203**(1): p. 181-191.
11. Seeber, M., et al., *EEG beta suppression and low gamma modulation are different elements of human upright walking*. Frontiers in Human Neuroscience, 2015. **9**: p. 1-9.
12. Bradford, J.C., J.R. Lukos, and D.P. Ferris, *Electrocortical activity distinguishes between uphill and level walking in humans*. Journal of Neurophysiology, 2015. **115**(2): p. 958-966.
13. Wagner, J., et al., *Level of participation in robotic-assisted treadmill walking modulates midline sensorimotor EEG rhythms in able-bodied subjects*. Neuroimage, 2012. **63**(3): p. 1203-11.
14. Bulea, T.C., et al. *User-driven control increases cortical activity during treadmill walking: An EEG study*. in *Engineering in Medicine and Biology Society (EMBC), 2014 36th Annual International Conference of the IEEE*. 2014. IEEE.
15. Presacco, A., et al., *Neural decoding of treadmill walking from noninvasive electroencephalographic signals*. J Neurophysiol, 2011. **106**(4): p. 1875-87.
16. Luu, T.P., et al. *A closed-loop brain computer interface to a virtual reality avatar: Gait adaptation to visual kinematic perturbations*. in *2015 International Conference on Virtual Rehabilitation (ICVR)*. 2015.
17. Luu, T.P., et al., *Gait adaptation to visual kinematic perturbations using a real-time closed-loop brain-computer interface to a virtual reality avatar*. Journal of Neural Engineering, 2016. **13**(3): p. 036006.
18. Luu, T.P., et al. *EEG-based Brain-Computer Interface to a Virtual Walking Avatar Engages Cortical Adaptation*. in *IEEE International Conference on Systems, Man, and Cybernetics*. 2017. IEEE.
19. Luu, T.P., et al., *Real-time EEG-based brain-computer interface to a virtual avatar enhances cortical involvement in human treadmill walking*. Scientific Reports, 2017. **7**(1): p. 8895.
20. Brantley, J.A., et al. *Noninvasive EEG Correlates of Overground and Stair Walking*. in *International Conference of the IEEE Engineering in Medicine and Biology Society*. 2016. IEEE.
21. Delorme, A. and S. Makeig, *EEGLAB: an open source toolbox for analysis of single-trial EEG dynamics including independent component analysis*. J Neurosci Methods, 2004. **134**(1): p. 9-21.
22. Gwin, J.T., et al., *Electrocortical activity is coupled to gait cycle phase during treadmill walking*. Neuroimage, 2011. **54**(2): p. 1289-96.
23. Bulea, T.C., et al., *Prefrontal, posterior parietal and sensorimotor network activity underlying speed control during walking*. Frontiers in Human Neuroscience, 2015. **9**: p. 247.
24. Luu, T.P., et al., *An individual-specific gait pattern prediction model based on generalized regression neural networks*. Gait & Posture, 2014. **39**(1): p. 443-448.
25. Luu, T.P., et al., *A closed-loop brain computer interface to a virtual reality avatar: Gait adaptation to visual kinematic perturbations*. 2015 International Conference on Virtual Rehabilitation (ICVR), 2015: p. 30-37.
26. Presacco, A., et al., *Neural decoding of treadmill walking from noninvasive electroencephalographic signals*. Journal of neurophysiology, 2011. **106**(4): p. 1875-1887.
27. Li, Z., et al., *Unscented Kalman filter for brain-machine interfaces*. PloS one, 2009. **4**: p. e6243.
28. Julier, S.J. and J.K. Uhlmann. *New extension of the Kalman filter to nonlinear systems*. 1997.
29. Luu, T.P., et al. *Unscented Kalman Filter for Neural Decoding of Human Treadmill Walking from Non-invasive Electroencephalography*. in *2016 38th Annual International Conference of the IEEE Engineering in Medicine and Biology Society (EMBC)*. 2016. IEEE.
30. Luu, T.P., et al., *Gait adaptation to visual kinematic perturbations using a real-time closed-loop brain-computer interface to a virtual reality avatar*. Journal of Neural Engineering, 2016. **13**(3): p. 036006.
31. Luu, T.P., et al. *A closed-loop brain computer interface to a virtual reality avatar: Gait adaptation to visual kinematic perturbations*. in *Virtual Rehabilitation Proceedings (ICVR), 2015 International Conference on*. 2015. IEEE.
32. Li, Z., et al., *Unscented Kalman filter for brain-machine interfaces*. PloS one, 2009. **4**(7): p. e6243.
33. Gwin, J.T., et al., *Removal of movement artifact from high-density EEG recorded during walking and running*. Journal of neurophysiology, 2010. **103**(6): p. 3526-3534.
34. Kilicarslan, A., R.G. Grossman, and J.L. Contreras-Vidal, *A robust adaptive denoising framework for real-time artifact removal in scalp EEG measurements*. J Neural Eng, 2016. **13**(2): p. 026013.
35. Paluš, M., *Nonlinearity in normal human EEG: cycles, temporal asymmetry, nonstationarity and randomness, not chaos*. Biological Cybernetics, 1996. **75**(5): p. 389-396.
36. Stam, C.J., *Nonlinear dynamical analysis of EEG and MEG: review of an emerging field*. Clinical Neurophysiology, 2005. **116**(10): p. 2266-2301.
37. Orsborn, A.L., et al., *Closed-loop decoder adaptation shapes neural plasticity for skillful neuroprosthetic control*. Neuron, 2014. **82**(6): p. 1380-93.
38. Orsborn, A.L., et al., *Closed-loop decoder adaptation on intermediate time-scales facilitates rapid BMI performance improvements independent of decoder initialization conditions*. IEEE Trans Neural Syst Rehabil Eng, 2012. **20**(4): p. 468-77.
39. Ganguly, K. and J.M. Carmena, *Neural correlates of skill acquisition with a cortical brain-machine interface*. Journal of Motor Behavior, 2010. **42**(6): p. 355-360.